Mesoscopic Coarse-Grained Simulations of Hydrophobic Charge Induction Chromatography (HCIC) for Protein Purification

Gaobo Yu, Jie Liu, and Jian Zhou

School of Chemistry and Chemical Engineering, Guangdong Provincial Key Lab for Green Chemical Product Technology, South China University of Technology, Guangzhou 510640, P.R. China

DOI 10.1002/aic.14805

Published online April 8, 2015 in Wiley Online Library (wileyonlinelibrary.com)

Mesoscopic coarse-grained simulations are adopted to investigate interfacial mechanisms of hydrophobic charged induction chromatography for protein purification by regulating pH. Simulations results indicate that: (i) lysozyme can be adsorbed mainly with "top end-on" and "bottom end-on" orientation on hydrophobic surfaces, dominated by the two hydrophobic regions located at both ends of lysozyme's long axis. Elution from the "top end-on" orientation is more difficult than that from the "bottom end-on" orientation; (ii) a higher ligand density can get a faster adsorption rate and stronger adsorption. Interestingly, the effect of ligand density on the desorption is mainly determined by the distribution probability of the positively charged groups of ligands; (iii) a higher ionic strength can lead to a wider orientation distribution, a stronger adsorption and a lower elution rate. This work might provide an efficient way to optimize the operating conditions and designing novel ligands. © 2015 American Institute of Chemical Engineers *AIChE J*, 61: 2035–2047, 2015

Keywords: protein purification, hydrophobic charged induction chromatography, protein adsorption, molecular simulation, coarse-graining, protein orientation

Introduction

Hydrophobic charge induction chromatography (HCIC)[1,2] is a new type of mixed-mode chromatography by regulating pH, in which the hydrophobic attraction controls protein adsorption whereas the electrostatic repulsion regulates protein desorption. HCIC has stimulated research interests in protein purification,[3–5] especially for the separation and purification of antibodies.[6–11] Compared with the hydrophobic interaction chromatography (HIC), HCIC can achieve a higher ligand density for higher separation capacity.[2] The selectivity of HCIC is relatively better than that of ion exchange chromatography, which is almost close to that of affinity chromatography (AC).[8,9] Moreover, HCIC has an advantage of low cost of ligand over AC.[8,9] To illuminate the HCIC process, some experimental studies,[2,4–7,11–14] a corresponding theoretical model[3] and computational researches[16–18] have been performed. However, the internal mechanisms of HCIC are still far from being completely understood at the molecular level.

One promising approach which provides the molecular insight into HCIC is molecular simulation.[19–31] It can directly investigate the dynamic process of protein adsorption and/or desorption at the microscopic level.[32] Recently, Wang et al.[33] performed a combination of molecular docking and atomistic molecular dynamics (MD) simulations to verify the separation mechanism of HCIC. Subsequently, they[34,35] explored the interactions between 4-mercaptoethylpyridine (MEP) ligand and Fc fragment of IgG, they also investigated the effects of the ligand structure and pH. Their simulation is in the nanosecond time scale. In addition, Zhang and Sun[36–39] investigated the dynamic process of HCIC and protein conformational transition within adsorbent by coarse-grained molecular dynamics (CGMD) simulations. They attempted to study the influences of salt, pH and ligand density.

Recently, Wei et al.[40,41] indicated out the adsorption/desorption behaviors of lysozyme on polyethylene surfaces. They proposed that the long simulation was needed in order to gain a complete understanding of the protein adsorption process. Because of this, we[42] used a mesoscopic coarse-grained method, based on the MARTINI force field for protein[43,44] and the big multipole water (BMW) model,[45,46] to study protein adsorption. This method can break the bottleneck of traditional MD simulation in space and time scales and can preserve basic structural detail of proteins. It is an attractive alternative to the atomistic model. Meanwhile, this simulation strategy can be applied for giving an insight into the mechanisms of HCIC.

In this work, we primarily aims to understand the interfacial mechanisms of HCIC at the molecular level, the adsorption/desorption behaviors of lysozyme on MEP are explored by the mesoscopic CGMD method. We adopt six initial orientations (i.e., six faces of lysozyme toward the

Correspondence concerning this article should be addressed to J. Zhou at jianzhou@scut.edu.cn

MEP ligand surface, respectively) of lysozyme for each system. Additionally, the influence of ionic strengths and ligand densities are taken into account for the internal mechanism.

Computation Methods

Force fields

All systems were simulated by the BMW-MARTINI force field,[46] which was developed based on the MARTINI (version 2.1) force field[43,44] and BMW water model.[45]

Moreover, in the BMW-MARTINI force field,[46] the type AC_1 and AC_2 in the original MARTINI[43,44] are replaced by C_1 and C_2; the original MARTINI Q_a is replaced by AQ_a for anions (Cl^-) and peptide C-ter; new subtypes are added for amino acids to introduce additional flexibility: RQ_d for guanidinium group in Arginine and AQ_a for aspartate and glutamate. Additionally, SQd is defined for the positively charged group in ring structures.

The potential energy (U_{tot}) (Eq. 1) is comprised of van der Waals (VDW) interaction energy (U_{vdw}) and electrostatic interaction energy (U_{ele}).

$$U_{tot} = U_{vdw} + U_{ele} \tag{1}$$

In the original MARTINI force field,[43,44] VDW interaction energy is calculated by Lennard–Jones potential (Eq. 2) model

$$U_{vdw} = 4\varepsilon_{ij}\left[\left(\frac{\sigma_{ij}}{r}\right)^{12} - \left(\frac{\sigma_{ij}}{r}\right)^{6}\right] \tag{2}$$

while in BMW-MARTINI force field,[45,46] a modified form of the Born–Mayer–Huggins (BMH)[47,48] potential (Eq. 3) is used to describe VDW interaction

$$U_{vdw} = \frac{\varepsilon}{1-\frac{f}{a}-\frac{6-f}{12}}\left\{\frac{6-f}{12}\left(\frac{r_m}{r}\right)^{12} - \left(\frac{r_m}{r}\right)^{6} + \frac{f}{a}\exp\left[a\left(1-\frac{r}{r_m}\right)\right]\right\} \tag{3}$$

In addition to the VDW interaction, charged groups interact via a shifted Coulombic potential energy function (Eq. 4) in the original MARTINI force field; while electrostatic interactions in the BMW-MARTINI model are calculated by the Particle-Mesh-Ewald (PME)[49,50] method

$$U_{ele} = \frac{q_i q_j}{4\pi\varepsilon_0\varepsilon_1 r} \tag{4}$$

It should be stressed herein that the original MARTINI force field[43,44] utilizes a relative dielectric constant (ε_1) of 15 for screening electrostatic interactions and consequently the original MARTINI force field may be less accurate to describe interactions between charged species. While in BMW-MARTINI model,[45,46] ε_1 is adjusted to 1.3.

Protein model and force fields

Lysozyme, a basic protein with low molecular weight and ellipsoid shape, has long been used as a model protein to study the enzyme kinetics, spatial conformation and protein purification.[5,24,39–42,51–53] Here, the atomistic structure of lysozyme crystal is taken from Protein Data Bank (PDB code: 1HEL) and is shown in Figure 1a. The CG structure of lysozyme is shown in Figure 1b. The backbone structure, main chemical properties of side-chains and secondary structures of lysozyme are preserved after CG mapping by the MARTINI model.[44,54]

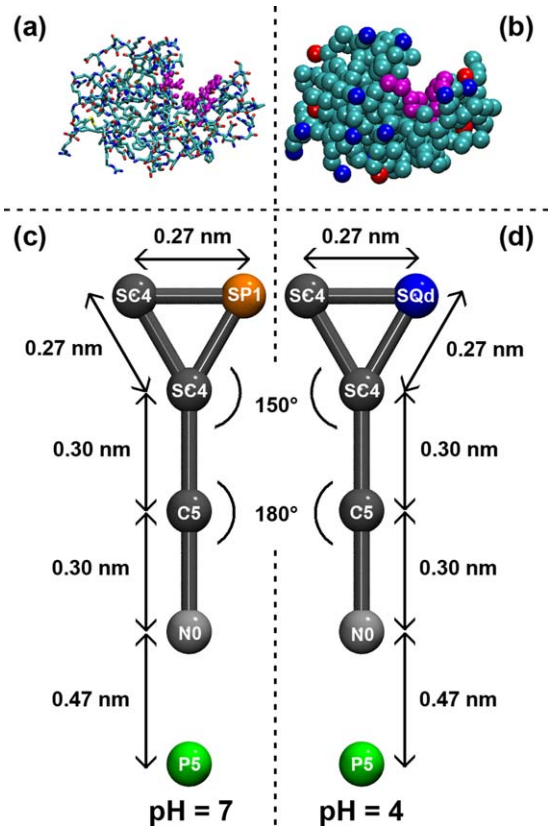

Figure 1. Structural models of lysozyme: (a) atomistic model, (b) CG model; and 4-mercaptoethylpyridine (MEP) ligand: (c) CG model at pH 7.0, (d) CG model at pH 4.0.

The positively charged atoms/beads are presented in blue and that negatively charged atoms/beads are presented in red. The magenta part is for the active cleft of lysozyme and the cyan atoms/beads are for the remainder part. The bead containing nitrogen of MEP ligand (N bead) is denoted by orange (pH 7.0) and by blue (pH 4.0). The hydrophobic beads of MEP ligand are colored in gray. The green is for the matrix (agarose). The same coloring scheme of lysozyme and adsorbent are used throughout the manuscript. [Color figure can be viewed in the online issue, which is available at wileyonlinelibrary.com.]

In this work, we do not aim to investigate the protein conformation. Thus, the elastic network constraint ELNEDYN[55] was used to maintain the relative stable conformation of lysozyme during simulations. The protonation states of lysozyme residues at different pH values were determined by PDB2PQR 1.9.0 (http://nbcr-222.ucsd.edu/pdb2pqr_1.9.0),[56] as shown in Figure 2. That is to say, the net charges of lysozymes are +8 e and +14 e at pH 7.0 and pH 4.0, respectively.

HCIC adsorbent model

As the actual diameter of adsorbent pore in HCIC is much larger than lysozyme's effective diameter, the HCIC adsorbent pore can be simplified as a planar matrix when investigating the adsorption and desorption behaviors of lysozyme on it. Here, to model the HCIC adsorbent, a series of MEP ligands are fixed to the agarose matrix by the N0 beads in

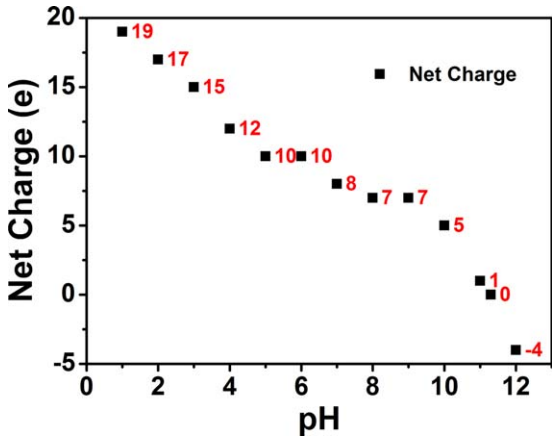

Figure 2. The net charge of lysozyme as a function of pH.

[Color figure can be viewed in the online issue, which is available at wileyonlinelibrary.com.]

planar, as shown in Figures 1 and 3. To mimic the chemical property of the HCIC adsorbent surface, a simplified processing is taken by the four-to-one mapping (on average four heavy atoms are represented by a single interaction center).[43] The simplified schemes for MEP monomer in this work are given in Figures 1c, d. As we know, the MEP ligand[2] is neutral at pH 7.0 and is positively charged at pH 4.0. The major difference is the protonation state of the N bead which represents for the nitrogen of MEP monomer. In each monomer, the N bead is represented by the polar SP1 bead at pH 7.0 (Figure 1c), while it is represented by the charged bead SQd (+1 e) at pH 4.0 which is named as the N^+ bead (Figure 1d). The bond lengths and angles of MEP monomer are shown in Figure 1. As the groups of MEP monomer are basically in a straight line,[33] thus the angle (∠SC4-C5-N0) is defined as 180°. The three beads on the ring are in the form of an equilateral triangle. Therefore, the angles (∠C5-SC4-SC5 and ∠C5-SC4-SP1) should be 150°. It should be noted that the N0 beads are fixed during the whole simulations to imitate the HCIC adsorbent. In additions, the bond lengths of MEP monomer are assigned according to the public profiles (i.e., MARTINI_v2.1_aminoacids.itp and MARTINI_v2.1_BMW.itp). By comparing the amino acids (i.e., Tyr, His, Phe, and Trp) with the ring, we can figure out that the bond lengths in the ring of MEP monomer (SC4-SC4, SC4-SP1, and SC4-SQd) are all 0.27 nm. Meanwhile, by comparing the levels of LJ interaction, we can consider that it is suitable to determine 0.30 nm as the bond lengths for both SC4-C5 and C5-N0. Finally, the bond length between the MEP ligand and the agarose plane (N0-P5) is set at 0.47 nm, because of the equilibrium distance between molecules in MARTINI force field is around 0.47 nm. Furthermore, four kinds of ligand density surfaces (0.74, 1.47, 2.21, and 2.95 μmol/m^2) are shown in Figure 3.

Simulation details

CGMD simulations in NVT ensemble were performed to examine the adsorption and desorption behaviors of lysozyme in HCIC using the GROMACS 4.5.5 package.[57] Compromised between computational resources and computational efficiency, in each system, six initial orientations of lysozyme (i.e., six faces of lysozyme toward the MEP ligand surface, respectively)[24] were taken into account and were shown in Figure 4a. The initial gap between the lysozyme and the MEP ligand surface is 1.0 nm (Figure 4a). Meanwhile, the influence of ionic strengths (0.05, 0.15, and 1.00 M) was also investigated. It is worth noting that, because of the smoothed energy barrier in the MARTINI force field, the effective time that the system goes through is four times longer than the simulation sampling time.[58] A 20 fs time step was used to integrate the equations of motion with the half leap-frog algorithm. 1.0 μs CGMD simulation was performed for each system. The simulation box size is 6.84 × 7.90 × 13.25 nm^3 and the water density in this work is about 1.041 × 10^3 kg/m^3, which well agrees with that of 1.047 × 10^3 kg/m^3 by Wu et al.[45] The neighbor list was updated every 10 steps with a cutoff 1.4 nm. PME with a spacing of 0.2 nm and $\varepsilon_r = 1.3$ were applied for electrostatics. For all LJ interactions, $r_{shift} = 0.9$ nm and $r_{cut} = 1.2$ nm; while the switch scheme ($r_{shift} = 0.9$ nm and $r_{cut} = 1.4$ nm) was used for water–water VDW interactions. The initial velocities of beads were generated based on the Maxwell distribution at the simulated temperature, which is controlled at 300 K by the Berendsen method[59] with a time constant of 0.2 ps. Other simulation parameters used in this work are the same as those in previous BMW-MARTINI works.[42,45,46] For structure and electrostatic potential visualization, the visual molecular dynamics (VMD)[60] and chimera[61] programs are used.

Results and Discussion

Here, the interfacial adsorption and desorption mechanisms of HCIC at different pH values are explained from three different aspects: orientation, ligand density and ionic strength. Results are shown in Figures 4–15.

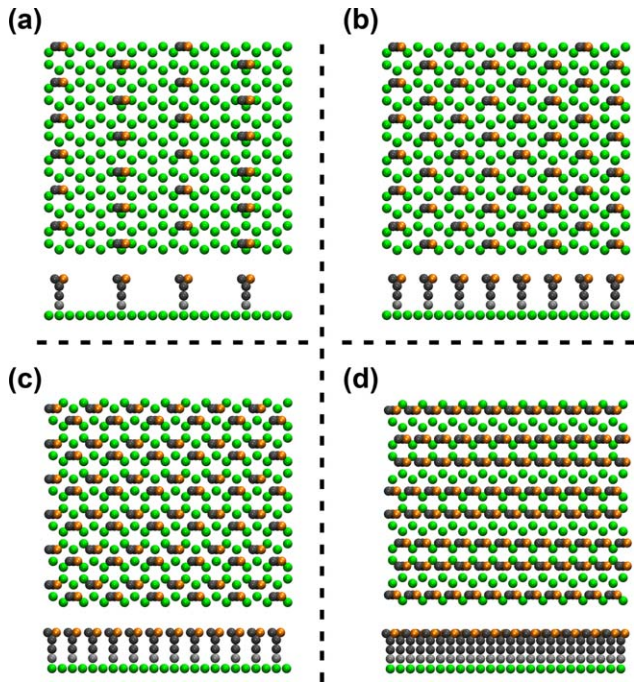

Figure 3. Top view and side view of surfaces at four kinds of ligand densities: (a) 0.74 μmol/m^2, (b) 1.47 μmol/m^2, (c) 2.21 μmol/m^2, (d) 2.95 μmol/m^2.

[Color figure can be viewed in the online issue, which is available at wileyonlinelibrary.com.]

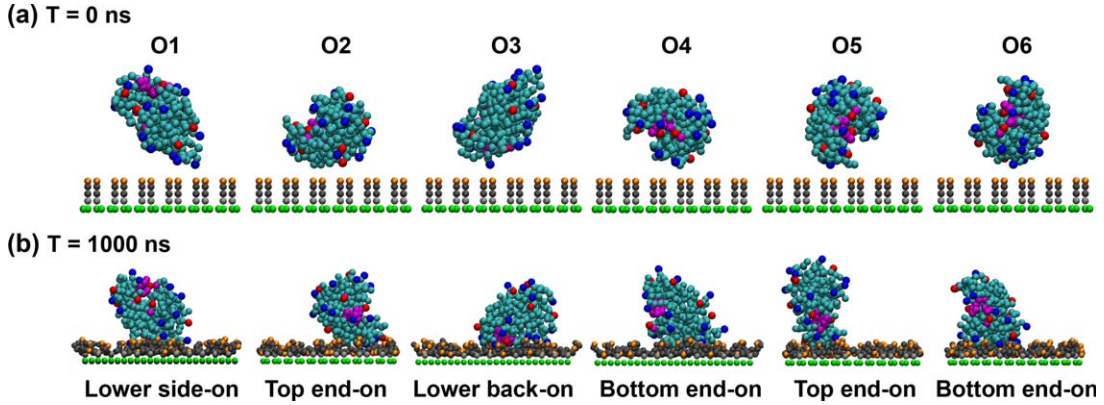

Figure 4. At pH 7.0, ligand density 2.21 μmol/m^2 and ionic strength 0.15 M, configurations of lysozyme orientations on the HCIC adsorbent.

(a) $t = 0$ ns, six different initial orientations (O1–O6) (i.e., six faces of lysozyme toward the MEP ligand surface, respectively); (b) $t = 1000$ ns, the corresponding adsorption orientations for O1–O6. Water and ion beads are not shown. [Color figure can be viewed in the online issue, which is available at wileyonlinelibrary.com.]

Orientation

In this section, as shown in Figures 4–8, the adsorption and desorption of lysozyme (O1–O6) in HCIC at the ligand density of 2.21 μmol/m^2 and the ionic strength of 0.15 M will be presented and discussed.

Our previous work[42] indicated that the preferred orientation of the same protein is different at different conditions. For the initial orientation of lysozyme on the MEP ligand surface, six different initial orientations (O1–O6) of lysozyme are considered and are shown in Figure 4a. For the adsorption process of HCIC at pH 7.0, the corresponding adsorbed states of lysozyme (O1–O6) on the HCIC adsorbent are displayed in Figure 4b. We can see a clear tendency that lysozyme prefers to adsorb with end-on orientation (the principal axis of lysozyme is almost parallel to the surface normal) on the MEP ligand surface no matter from any initial orientation. Furthermore, we investigate the orientation distributions of lysozymes (O1–O6) adsorbed on the HCIC adsorbent, as shown in Figure 5. In an early work,[24] the orientation angle (θ) was used to quantitatively characterize the orientation of adsorbed proteins on surfaces. It is defined as the angle between the unit vector normal to the surface and the unit vector along the dipole of a protein. The cos values of this angle were calculated for each possible orientation. According to the statistical results shown in Figure 5, we can figure out that the favored orientation of lysozyme on the MEP ligand surface is "end-on" orientation, which is consistent with the experiment result.[62] However, this "end-on" orientation can be further divided into two categories (i.e., "top end-on" orientation and "bottom end-on" orientation). Initial orientations (O2, O3, and O5) tend to form "top end-on" orientation ($\cos\theta > 0.60$), while initial orientations (O1, O4, and O6) tend to adsorb with "bottom end-on" orientation ($\cos\theta < -0.60$). Since MEP ligands are neutral at the adsorption pH (pH = 7.0), the electrostatic interactions between lysozyme and ligands are weak, lysozyme adsorption is driven by hydrophobic interactions.[2] In our simulations, there is no electrostatic interaction between lysozyme and the MEP ligand surface during the adsorption process. That is to say, the adsorption of lysozyme on the MEP ligand surface is driven by the hydrophobic attraction. The molecular docking work by Wang et al.[33] indicated that MEP ligand tended to bind on the hydrophobic region of Fc of antibody. Thus, based on Figures 4 and 5, we can infer that the hydrophobic regions on the lysozyme surface might locate at both ends of lysozyme's long axis. As a result, the two hydrophobic regions can drive lysozyme to adsorb onto the MEP ligand surface with either "top end-on" or "bottom end-on" orientations. The detailed information about the two hydrophobic regions will be further discussed below.

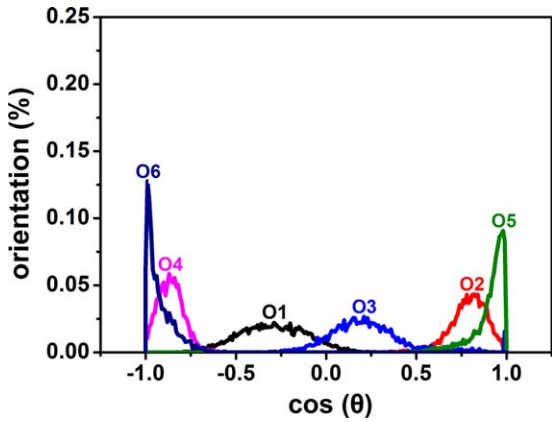

Figure 5. At pH 7.0, ligand density 2.21 μmol/m^2 and ionic strength 0.15 M, orientation distributions of lysozyme adsorbed on the HCIC adsorbent from different initial orientations (O1–O6).

Color representations: black (O1); red (O2); blue (O3); magenta (O4); olive (O5); navy (O6). [Color figure can be viewed in the online issue, which is available at wileyonlinelibrary.com.]

Figure 6 displays the min-distance between lysozymes (O1–O6) and the HCIC adsorbent during the desorption process. It can be seen that lysozymes (O4 and O6) which have the "bottom end-on" orientation and lysozymes (O1 and O3) which do not have the "end on" orientations can be successfully desorbed from the HCIC adsorbent; while lysozymes (O2 and O5) which have the "top end-on orientation" fail in desorption. As we know, the MEP ligand turns to be positively charged (+1 e) when the pH value is less than 4.8.[2] When the pH value is 4.0, each MEP ligand will carry a positive charge. As a result, the HCIC adsorbent can show a surface charge density up to 0.213 C/m^2. Meanwhile, lysozyme is positively charged (+14 e) at the desorption pH.

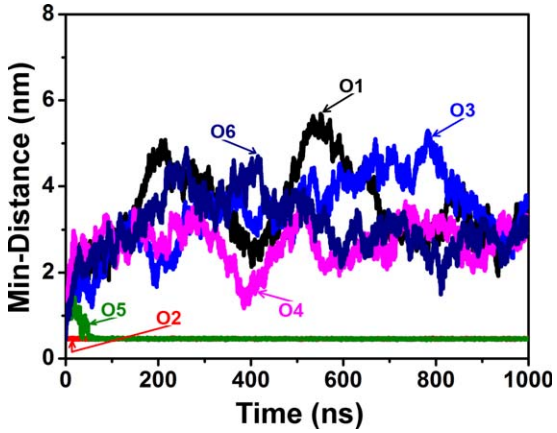

Figure 6. At pH 4.0, ligand density 2.21 μmol/m^2 and ionic strength 0.15 M, min-distances between lysozyme (O1–O6) and the HCIC adsorbent during the desorption process.

Color representations: black (O1); red (O2); blue (O3); magenta (O4); olive (O5); navy (O6). [Color figure can be viewed in the online issue, which is available at wileyonlinelibrary.com.]

Therefore, lysozymes (O1–O6) are almost dissociated by the strong electrostatic repulsion except for the O2 case. In addition, the lysozyme (O5) readsorbs quickly ($T \approx 48.6$ ns) after desorption and still adsorbs with a "top end-on" orientation. By comparing the "top end-on" and "bottom end-on" orientations, we find out that desorption from the "top end-on" orientation is more difficult than that from the "bottom end-on" orientation. To further support the conclusions above, the total potential energies (U_{tot}) between lysozyme and MEP ligand surface have been listed in Table 1 for each system in Figure 6. When solution pH is 7.0 for adsorption, it is clear that the U_{tot} of cases (O2, O3, and O5) for attraction are obviously stronger than those of cases (O1, O4, and O6). However, when the pH decreases to 4.0 for desorption, the U_{tot} of cases (O2, O3, and O5) for repulsion are much weaker than those of cases (O1, O4, and O6). Especially, the U_{tot} of cases (O2) is negative at desorption pH (Table 1). That is to say, in cases (O2), the electrostatic repulsion can not beat the hydrophobic attraction, which leads to the failure of dissociation (red curve in Figure 6). As discussed above, initial orientations (O2, O3, and O5) tend to form "top end-on" orientation, while initial orientations (O1, O4, and O6) tend to adsorb with "bottom end-on" orientation. Therefore, it is straightforward that lysozyme desorption from the "top end-on" orientation is more difficult than that from the "bottom end-on" orientation. As shown in our previous work,[42] lysozyme has a major positive potential region around Arg128. Thus, we can infer that the "top end-on" orientation is far away from the major positive potential region, leading to the relatively weaker electrostatic repulsion. To validate the interfacial mechanisms of HCIC, we further explore the key residues of lysozyme (Figure 7) and the dominant regions located on the surface of lysozyme for adsorption and desorption (Figure 8).

The contact map of key residues is plotted in Figure 7 by monitoring the distance between each bead of lysozyme and the top layer of the surface along the z-direction.[29] When such distance is less than 0.5 nm, the residue containing the corresponding bead is considered to be in contact with the surface and is plotted in the map. As shown in Figure 7, the contact maps of lysozymes (O1–O6) on the HCIC adsorbent can be divided into two categories, which are consistent with the tendency of the orientation distributions of lysozymes (O1–O6) (see Figure 5). That is to say, lysozymes (O1, O4, and O6) tend to adsorb with the "bottom end-on" orientation on the HCIC adsorbent; meanwhile, the key residues of lysozymes (O1, O4, and O6) (Figures 7a, d, f) always appear at the terminal residues of lysozyme. However, lysozymes (O2, O3, and O5) tend to have the "top end-on" orientation and their key residues (Figures 7b, c, e) concentrate on the middle residues of lysozyme. By comparing Figures 7b, c, e, it can be seen that lysozyme (O2) has more key residues and wider distribution of key residues than lysozymes (O3 and O5). This indicates that lysozyme (O2) has a more stable adsorption on the HCIC adsorbent than lysozymes (O3 and O5). This is the reason why lysozyme (O2) fails in the whole desorption process (red curve in Figure 6).

As for the driving mechanism of HCIC, the dominant hydrophobic regions and positive potential regions of lysozyme are displayed in Figure 8. Figure 8a shows the hydrophobic surface of lysozyme at the adsorption pH (pH = 7.0) and highlights its two hydrophobic regions. Figure 8b displays the electrostatic surface of lysozyme at the desorption pH (pH = 4.0) and stands out its two positive potential regions. Finally, we also list the main residues of each region at the bottom of Figure 8. As shown in Figure 8, the existence of some hydrophobic regions on both ends of lysozyme's long axis is consistent with our previous discussion, so lysozyme could be driven to adsorb with "top end-on" or "bottom end-on" orientations. Moreover, with Figures 7 and 8a, we can further suggest that the "bottom end-on" orientation is driven by the hydrophobic region A and the "top end-on" orientation is dominated by the hydrophobic region B for lysozyme adsorption on the strong hydrophobic MEP ligand surface at pH 7.0. Therefore, as described above, our simulation results demonstrate the driven mechanism for the adsorption of lysozyme in HCIC.

Additionally, the hydrophobicity of the hydrophobic region B is stronger than region A since it owns 10 more hydrophobic residues (Figure 8a). Obviously, this is one reason why lysozyme desorption from the "top end-on" orientation is more difficult than that from the "bottom end-on" orientation (Figure 6). Meanwhile, we can figure out another reason of the desorption mechanism in HCIC from Figure 8b. According to Figure 8b, 13 positive residues (Lys1, Arg5, Lys13, Arg14, His15, Arg21, Lys33, Lys96, Lys97, Arg114, Lys116, Arg125, and Arg128) of lysozyme are gathered in the positive potential region C, which makes it the dominating center for lysozyme desorption on the MEP ligand surface (positively charged at pH 4.0). By contrast,

Table 1. Total Potential Energies (U_{tot}) Between Lysozyme and MEP Ligand Surface at Adsorption pH and Desorption pH for Systems in Figure 6

Orientation	pH = 7.0 U_{tot} (kJ/mol)	pH = 4.0 U_{tot} (kJ/mol)
O1	−67.8	80.7
O2	−104.7	−16.8
O3	−88.3	16.5
O4	−73.5	81.3
O5	−96.6	2.8
O6	−75.6	86.4

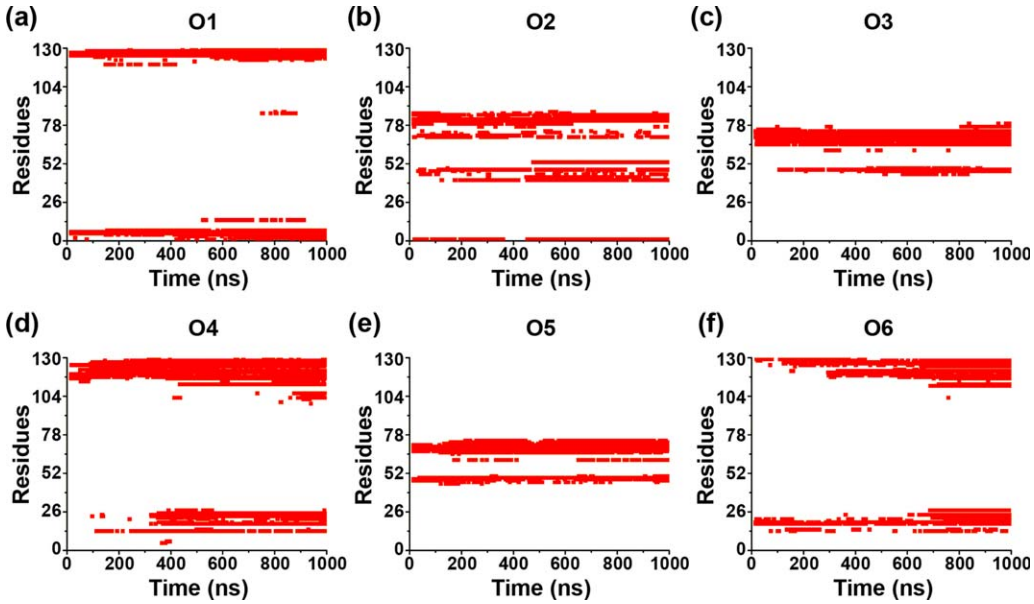

Figure 7. At pH 4.0, ligand density 2.21 μmol/m^2 and ionic strength 0.15 M, the key residues of lysozyme adsorbed on the HCIC adsorbent from different initial orientations (O1–O6) during the adsorption process.

[Color figure can be viewed in the online issue, which is available at wileyonlinelibrary.com.]

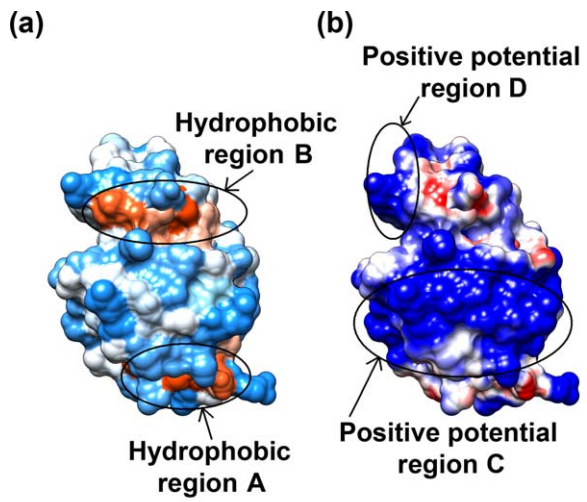

Hydrophobic region A:
Cys6, Leu25, Val120, Ala122, Trp123, Ile124, Cys127, Leu129.

Hydrophobic region B:
Ala42, Ile55, Leu56, Ile58, Trp62, Trp63, Cys64, Pro70, Leu75, Cys76, Ile78, Pro79, Cys80, Ala82, Leu83, Leu84, Ile88, Ala90.

Positive potential region C:
Lys1, Arg5, Lys13, Arg14, His15, Arg21, Lys33, Lys96, Lys97, Arg114, Lys116, Arg125, Arg128.

Positive potential region D:
Arg45, Arg61, Arg68, Arg73.

Figure 8. The dominant regions for lysozyme's adsorption and desorption on the HCIC adsorbent.

(a) The hydrophobicity surface of lysozyme at pH 7.0; (b) the electrostatic surface of lysozyme at pH 4.0. Color representations: orange (hydrophobic); cyan (hydrophilic); blue (positive); red (negative). [Color figure can be viewed in the online issue, which is available at wileyonlinelibrary.com.]

there are just 4 positive residues (Arg45, Arg61, Arg68, and Arg73) belong to the positive potential region D. Therefore, lysozyme can be dissociated by electrostatic repulsion more easily when the positive potential region C faces toward the MEP ligand surface. In sum, the hydrophobic interactions between the "bottom end-on" lysozyme and surface are weaker than that between the "top end-on" lysozyme and surface; however, the "bottom end-on" lysozyme can acquire stronger electrostatic repulsion than the "top end-on" lysozyme in the elution process. As a result, it is easier for lysozyme adsorbed with a "bottom end-on" orientation to elute from the HCIC resin than that with a "top end-on" orientation. Thus, the reason for those proteins failed in elution,[5,10,15] is that they adsorb with an unfavorable orientation. Consequently, lysozymes with suitable initial orientations (O1, O4, and O6) can mainly adsorb with the "bottom end-on" orientation, so they have faster elution rates in the actual operation.

Finally, it should be noted out that the electrostatic interaction has been enhanced by reducing the relative dielectric constant to 1.3 in the BMW-MARTINI force field.[45,46] Meanwhile, a much softer potential has been employed to describe the nonpolar component rather than the commonly used Lennard–Jones form in the original MARTINI.[45] However, the hydrophobic interaction is still overestimated in contrast to the experimental observations,[46] which would lead to a too strong adsorption of lysozyme on the MEP ligand surface. That is to say, this force field feature might be another reason for the failed desorption of lysozyme.

Ligand density effect

In this section, four different ligand densities (0.74, 1.47, 2.21, and 2.95 μmol/m^2) have been employed to investigate the effect of ligand density on the adsorption and desorption mechanism in HCIC. The corresponding simulation results of lysozyme (O2) at the ionic strength of 0.05 M are presented in Figures 9–11.

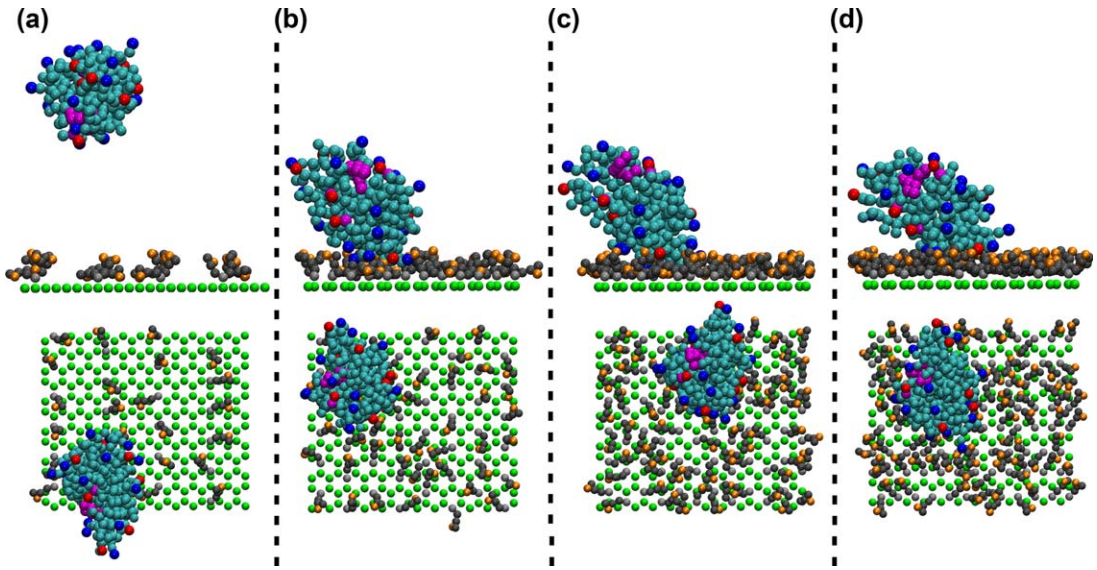

Figure 9. At pH 7.0 and ionic strength 0.05 M, the final conformations of lysozyme (O2) at four different ligand densities.

(a) 0.74 μmol/m^2, (b) 1.47 μmol/m^2, (c) 2.21 μmol/m^2, AND (d) 2.95 μmol/m^2. Water and ion beads are not shown. [Color figure can be viewed in the online issue, which is available at wileyonlinelibrary.com.]

Figure 9 shows the final conformations of lysozyme (O2) at the four different ligand densities after the adsorption process. Although the simulation time (1000 ns) is long enough, lysozyme fails to adsorb at the ligand density of 0.74 μmol/m^2 (Figure 9a). This is because that the coverage of ligand matrix is too low when the ligand density is 0.74 μmol/m^2, the hydrophobic interactions between lysozyme and the MEP ligand surface are not strong enough for adsorption. With the increase of the ligand density, more MEP ligands can be utilized as contact sites. Therefore, lysozyme can adsorb onto the MEP ligand surface stably at elevated ligand densities. These simulation results indicate that a higher ligand density is better for lysozyme adsorption, which is in agreement with the experimental results by Zhao et al.[12] They suggested that ligand density had a positive influence on protein adsorption.

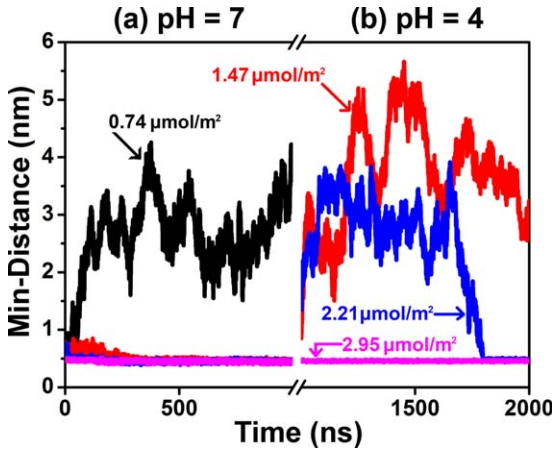

Figure 10. At ionic strength 0.05 M, min-distances between lysozyme (O2) and the HCIC adsorbent during the whole HCIC process.

(a) The first 1000 ns for adsorption; (b) the second 1000 ns for the desorption. Color representations: black (0.74 μmol/m^2); red (1.47 μmol/m^2); blue (2.21 μmol/m^2); Magenta (2.95 μmol/m^2). [Color figure can be viewed in the online issue, which is available at wileyonlinelibrary.com.]

To further demonstrate the effect of ligand density analyzed above, the evolution of the min-distance between lysozyme and ligand surfaces during the whole HCIC process are shown in Figure 10. From the first 1000 ns for the adsorption (Figure 10a), we can figure out that a high ligand density has a positive influence on the adsorption rate. At the low ligand density of 0.74 μmol/m^2, lysozyme keeps away from the MEP ligand surface during the adsorption process (black curve in Figure 10a). This is consistent with the discussion above. At higher ligand densities of 1.47, 2.21, and 2.95 μmol/m^2, the simulation time for stable adsorption is around 300, 175, and 130 ns (red, blue, and magenta curves in Figure 10a), respectively. This shows that higher ligand densities can make the lysozyme achieve stable adsorption in a shorter time. It also means that a higher ligand density has a positive effect on protein adsorption as previously discussed.

Figure 10b shows the evolution of min-distance of lysozyme to surface during the desorption process at pH 4.0 in another 1000 ns. When pH is switched from 7.0 to 4.0, lysozyme is immediately dissociated at the ligand densities of 1.47 and 2.21 μmol/m^2. However, at the ligand density of 2.21 μmol/m^2, after 800 ns, lysozyme adsorbs again (blue curve in Figure 10b). Additionally, at the highest ligand density of 2.95 μmol/m^2, lysozyme fails to dissociate from the ligand surface throughout the desorption process (magenta curve in Figure 10b). These results suggest that the rapid dissociation at the beginning of desorption process is induced by the sudden electrostatic repulsion. At the ligand densities of 1.47 and 2.21 μmol/m^2, the repulsive electrostatic interactions are stronger than the attractive hydrophobic interactions, which will lead to the rapid dissociation of lysozyme (red and blue curves in Figure 10b). Generally speaking, the ligand surface with the highest ligand density of 2.95 μmol/m^2 has the strongest repulsive electrostatic interactions to lysozyme. To our surprise, we cannot observe the rapid dissociation at the ligand density of 2.95 μmol/m^2 (magenta

Table 2. Total Potential Energies (U_{tot}) Between Lysozyme and MEP Ligand Surface at Adsorption pH and Desorption pH for Systems in Figure 10

Ligand Density (μmol/m^2)	pH = 7.0 U_{tot} (kJ/mol)	pH = 4.0 U_{tot} (kJ/mol)
0.74	0	/
1.47	−64.5	16.6
2.21	−98.6	11.0
2.95	−121.3	−28.5

curve in Figure 10b), since the highest ligand density (2.95 μmol/m^2) also leads to the highest hydrophobic attraction. Quantitatively, Table 2 lists the total potential energies (U_{tot}) between lysozyme and MEP ligand surface for each system in Figure 10. As ligand density increases (Table 2), the riseup of U_{tot} at adsorption pH indicates a strengthening in adsorption. It should be pointed out that only the U_{tot} of 2.95 μmol/m^2 case is negative at desorption pH (Table 2), since the hydrophobic attraction is too strong to be defeated by the electrostatic repulsion.

To further point out the inherent reason for this interesting phenomenon, the distribution probability of beads containing nitrogen atoms (N beads) around the interface are analyzed at the four different densities, as shown in Figure 11. We can find that the distribution probability curves at four densities all show double peaks. The first peaks at about 0.9 nm represent the N beads approaching to the matrix; while the second peaks at about 1.3 nm represent the N beads facing toward the bulk phase. Due to the distribution of N beads (Figure 11), the hydrophobic attraction and the electrostatic repulsion should be divided into two parts. One is from the MEP ligands in the first peak; the other is from the MEP ligands in the second peak. In addition, because the adsorbed lysozyme obviously has penetrated into the MEP ligands as displayed in Figure 9, thus the electrostatic repulsion from

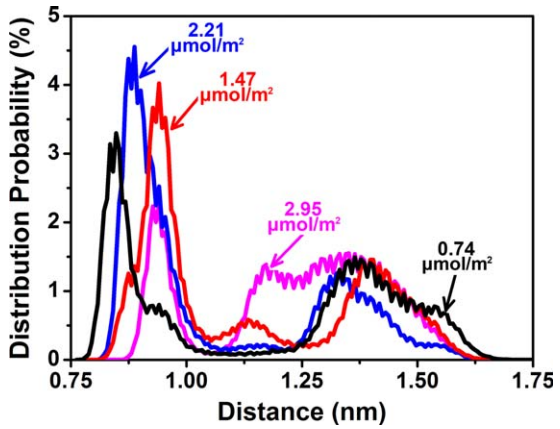

Figure 11. At pH 7.0 and ionic strength 0.05 M, distribution probability of beads containing nitrogen atoms at the four different densities.

Color representations: black (0.74 μmol/m^2); red (1.47 μmol/m^2); blue (2.21 μmol/m^2); Magenta (2.95 μmol/m^2). [Color figure can be viewed in the online issue, which is available at wileyonlinelibrary.com.]

the first peak are acting on the bottom of lysozyme, which effectively contributes to the desorption; whereas that from the second peak is ineffective. This is because the electrostatic repulsion from the second peak are lateral to lysozyme, thus these electrostatic repulsion surrounding lysozyme can counteract with each other. Moreover, a higher peak height of the second peak means a larger contract area between lysozyme and the MEP ligand surfaces, which would lead to stronger hydrophobic attraction.

Compared with the peaks shown in Figure 11, it is found that all peak heights of the first peaks raise up with the increase of ligand density except for the highest ligand

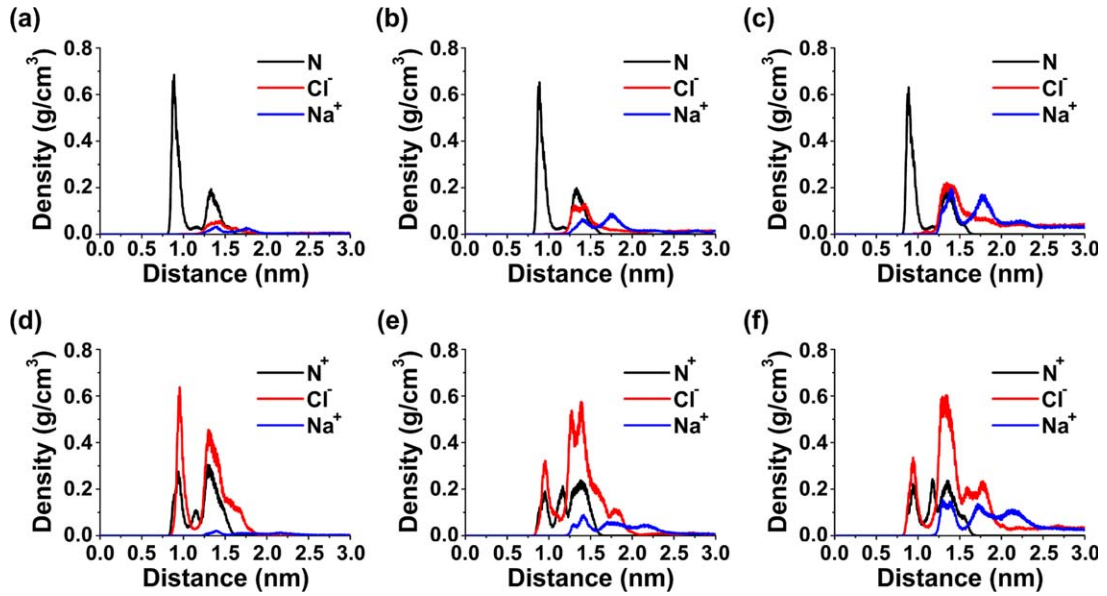

Figure 12. At ligand density 2.21 μmol/m^2, density distributions of the beads under three different ionic strengths after the adsorption process (a: 0.05 M, b: 0.15 M, c: 1.00 M) and the desorption process (d: 0.05 M, e: 0.15 M, f: 1.00 M).

Color representations: black (the beads containing nitrogen of MEP ligand); red (the beads of chloride ions); blue (the beads of sodium ions). [Color figure can be viewed in the online issue, which is available at wileyonlinelibrary.com.]

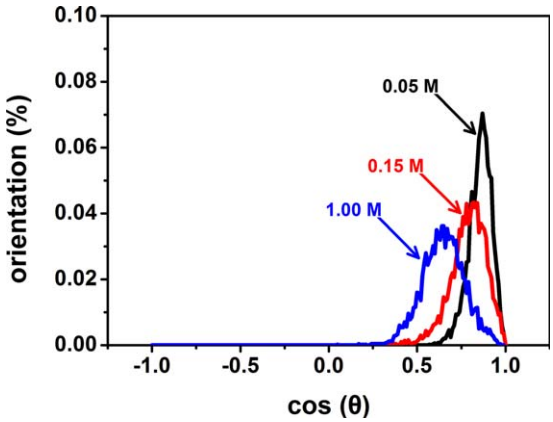

Figure 13. At pH 7.0 and ligand density 2.21 μmol/m^2, orientation distributions of lysozyme (O2) adsorbed on the HCIC adsorbent under three different ionic strengths.

Color representations: black (0.05 M); red (0.15 M); blue (1.00 M). [Color figure can be viewed in the online issue, which is available at wileyonlinelibrary.com.]

density of 2.95 μmol/m^2 (magenta curve in Figure 11). The tendency of the second peaks is just opposite with the first peaks especially at the ligand density of 2.95 μmol/m^2. As a result, the surface with the highest ligand density of 2.95 μmol/m^2 leads to a much stronger hydrophobic attraction than the other three surfaces with ligand densities of 0.74, 1.47, and 2.21 μmol/m^2; while the effective electrostatic repulsion is strongest at the second highest ligand density of 2.21 μmol/m^2. So the ligand density of 2.21 μmol/m^2 is the preferred ligand density to compromise hydrophobic attraction and electrostatic repulsion. That is to say, the distribution probability of N beads plays an important role in the interfacial mechanism of HCIC. In conclusion, faster elution rate can be obtained if more positively charged groups of HCIC ligands can concentrated on the first peak just as shown in Figure 11, which might be helpful to the optimization of operating conditions and the design of novel ligands.

Ionic strength effect

Here, we display a variety molecular details of lysozyme adsorption and desorption in HCIC, with special focus on the influence of ionic strength (IS). Three different ionic strengths (0.05, 0.15, and 1.00 M) are investigated by the mesoscopic CGMD simulations and the relevant results of lysozyme (O2) at the ligand density of 2.21 μmol/m^2 are summarized in Figures 12–15.

Figure 12 shows the interfacial density distributions at three different ionic strengths (0.05, 0.15, and 1.00 M) for the whole HCIC process. With the increase of IS for the adsorption process (Figure 12a–c), the higher IS still can make more ions to exist between lysozyme and MEP ligand surfaces although the adsorption is driven by the hydrophobic attraction. These interfacial ions can be considered as linkers between lysozyme and MEP ligands, which can promote the adsorption indirectly. Thus, the increase of IS can provide more probability for lysozyme to adsorb onto the MEP ligand surface, even if the adsorption orientation has a little deviation. That is to say, more interfacial ions can make wider orientation distributions, as displayed in Figure 13. Moreover, Figure 12 also shows that the center of the cosine values shifts from 1.0 to 0.5 gradually due to the increase of IS.

Furthermore, all key residues of lysozyme at three different ionic strengths (0.05, 0.15, and 1.00 M) are displayed for the adsorption (Figure 14a) and desorption (Figure 14b) processes. Compared with the contact maps of the three ionic strengths at pH 7.0 (Figure 14a), it can be clearly seen

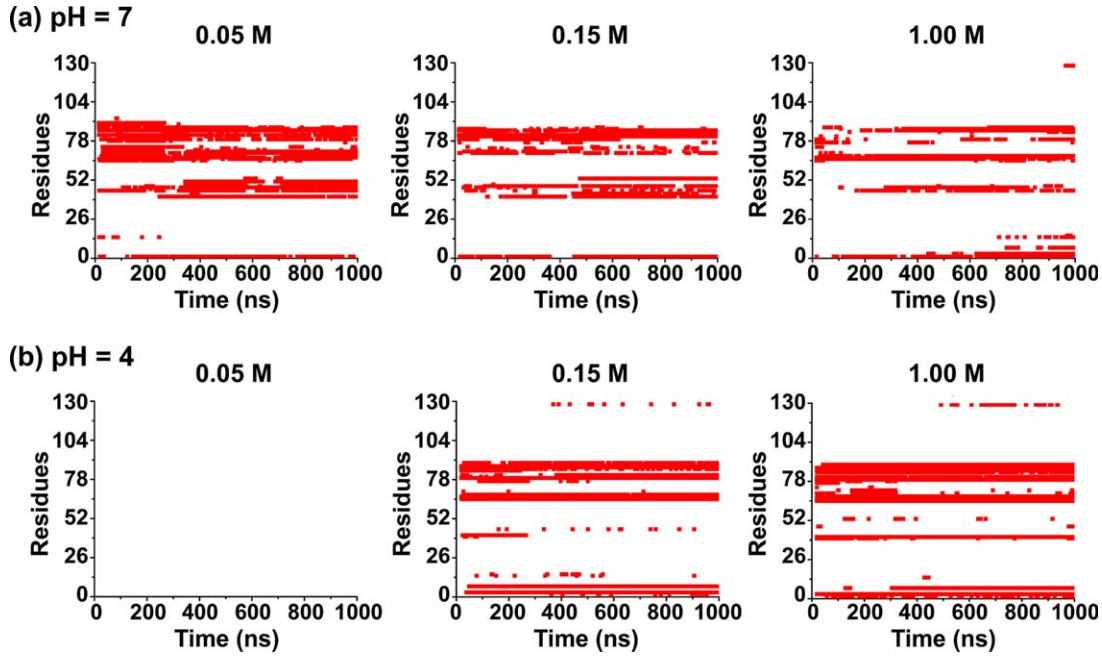

Figure 14. At ligand density 2.21 μmol/m^2, key residues of lysozyme adsorbed on the HCIC adsorbent under three different ionic strengths during the adsorption process (a) and the desorption process (b).

At the desorption pH (pH = 4.0), (b) is empty at ionic strength 0.05 M, which means there is no close contact. [Color figure can be viewed in the online issue, which is available at wileyonlinelibrary.com.]

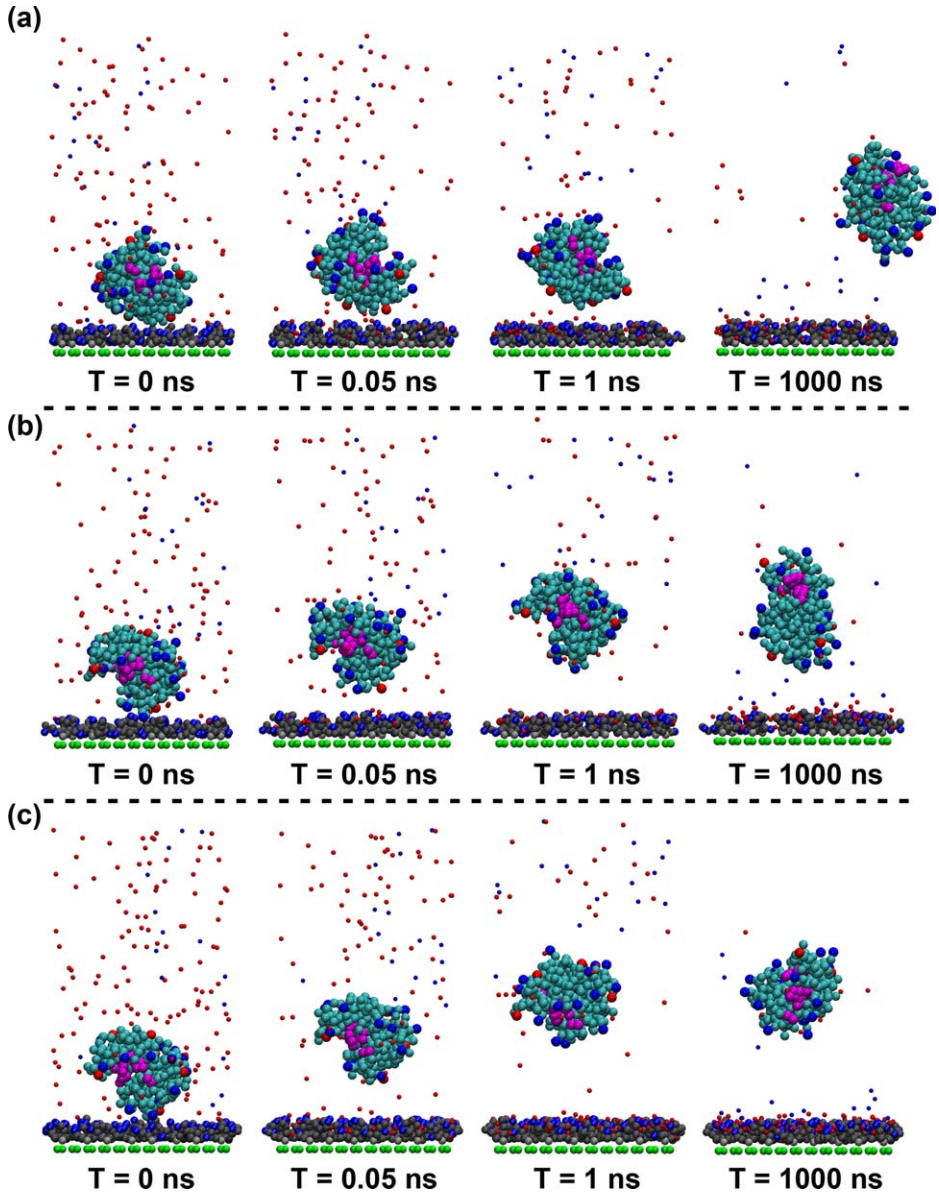

Figure 15. At ionic strength 0.15 M, conformations of lysozyme at four different time points (0, 0.05, 1, and 1000 ns) during the desorption process.

(a) Top end-on orientation at 1.47 μmol/m^2, (b) bottom end-on orientation at 1.47 μmol/m^2, (c) bottom end-on orientation at 2.21 μmol/m^2. Color representations: red (the beads of chloride ions); blue (the beads of sodium ions). [Color figure can be viewed in the online issue, which is available at wileyonlinelibrary.com.]

that the direct contacts between lysozyme and MEP ligands reduce with the riseup of IS. This is due to the existence of ions as discussed above, which can result in the indirect adsorption. However, the tendency is opposite for the contact maps of desorption (Figure 14b). That is to say, a higher IS leads to less direct contacts but more difficult dissociation from the MEP ligand surface. The primary reason for this phenomenon is also induced by the interfacial ions, especially by Cl^-. It should be pointed out that Cl^- is more inclined to appear near the interface while Na^+ tends to stay in the bulk,[42,63–65] which is consistent with that as shown in Figure 12, because the ionic hydration of Na^+ is stronger than that of Cl^-.[66] Therefore, due to the existence of interfacial ions, the electrostatic repulsive interactions can be offset by Cl^- ions, meanwhile there are competing interactions with Cl^- ions between interfacial Na^+ ions and the positively charged lysozyme (+14 e). That is to say, interfacial ions can weaken the electrostatic repulsion between lysozyme and MEP ligands. Additionally, the hydrophobic attraction can be intensified indirectly by interfacial ions. As mentioned above, the successful desorption is caused by that electrostatic repulsive interactions can beat hydrophobic attractive interactions. Thus, the desorption failure might due to interfacial ions. A higher IS induces more interfacial ions, thus the electrostatic repulsion would be weakened, which leads to a lower elution rate. As a result, the influence of IS on HCIC is mainly determined by the corresponding interfacial ions.

For the density distribution of initial state of desorption, that is, those of the final state of adsorption (Figures 12a–c), when compared with the final density distribution of desorption (Figures 12d–f), we find out that N beads have an

obvious shift toward the bulk, which is induced by interfacial Cl^- ions during the desorption process. Due to the shift of N beads, the contact between lysozyme and MEP ligands would increase significantly if lysozyme fails to dissociate at the beginning of desorption (Figure 14b). That is to say, the success or failure of desorption is almost determined at the initial stage, especially under the high ionic strength. Thus, to point out the internal reason visually, some lysozyme conformations at different desorption stages are shown in Figure 15. It can be seen that the dissociations from the HCIC adsorbent almost complete within a nanosecond. So, the rapid release of lysozyme is induced by the stronger electrostatic repulsion during the switch of pH (from 7.0 to 4.0). Meanwhile, for the same reason, positively charged MEP ligands at pH 4.0 can make negatively charged chloride ions in bulk to approach the surface with an extremely fast rate (see Figure 15). Thus, within the first nanosecond, the stronger electrostatic repulsive interactions have been greatly weakened by interfacial Cl^- ions, which is consistent with our previous work.[42] Compared with the density distributions shown in Figure 12, a higher IS induces more interfacial ions; meanwhile, it can make the instantaneous electrostatic repulsion more obvious. In conclusion, the dissociation of lysozyme is a quick process which almost happens at the initial stage of desorption as mentioned above. So in the actual elution operation, it is essential to avoid using those salts containing ions which are tend to concentrate at the adsorbent surface, such as Cl^-.

Furthermore, Figure 15 shows that as the desorption is successful, the desorption rate of "bottom end-on" orientation (Figure 15b) is faster than that of "top end-on" orientation (Figure 15a) thanks to the positive potential region C. From the "bottom end-on" orientation (Figures 15b, c), the higher the ligand density is, the faster the desorption rate in HCIC. These results are consistent with the discussions presented in previous two sections.

Conclusions

In this study, mesoscopic coarse-grained simulations based on BMW-MARTINI force field are utilized to reveal the interfacial mechanisms of HCIC by simulating the adsorption and desorption of lysozyme on MEP ligand surfaces at the mesoscopic microsecond time scale (2.0 μs). Four ligand densities (0.74, 1.47, 2.21, and 2.95 $\mu mol/m^2$) and three ionic strengths (0.05, 0.15 and 1.00 M) are considered to investigate the internal mechanisms in HCIC.

Simulation results indicate that: (i) from six different initial orientations, lysozyme can mainly adsorb with "top end-on" or "bottom en-on" orientations, which is driven by the two hydrophobic regions located at two ends of lysozyme's long axis; (ii) for the desorption in HCIC, the elution from the "top end-on" orientation is more difficult than that from the "bottom end-on" orientation; hydrophobic interactions between the "bottom end-on" lysozyme and the ligand surface are weaker than those between the "top end-on" lysozyme and the ligand surface; meanwhile, the "bottom end-on" orientation can acquire stronger electrostatic repulsion than the "top end-on" orientation during the elution process; (iii) for the adsorption in HCIC, a higher ligand density could result in a faster adsorption rate and stronger adsorption; a higher ionic strength can obtain a wider orientation distribution and a stronger adsorption; (iv) the effect of ligand density on the desorption of HCIC is mainly determined by the distribution probability of the positively charged groups of the HCIC ligands, that is, more these groups close to the matrix can lead a faster elution rate; (v) a higher ionic strength causes more interfacial ions, leading to a lower elution rate since the interfacial ions can weaken the electrostatic repulsion and intensify the hydrophobic attraction between lysozyme and ligands.

In general, mesoscopic CGMD simulation based on the BMW-MARTINI force field can be used to accurately explore the molecular insights of HCIC at the microsecond time scale, especially for the optimization of operating conditions and the design of novel ligands. Furthermore, these mesoscopic CGMD simulations are about 100 times faster than atomistic simulations. It is a more efficient approach that could be applied to understand the interfacial mechanisms of HCIC on the mesoscopic microsecond time scale.

Acknowledgments

Support from the National Key Basic Research Program of China (No. 2013CB733500), National Natural Science Foundation of China (Nos. 21376089, 91334202), Guangdong Science Foundation (No. S2011010002078, 2014A030312007) and the Fundamental Research Funds for the Central Universities (SCUT-2013ZM0073) are gratefully acknowledged. An allocation time from the SCUTGrid at South China University of Technology is gratefully acknowledged.

Literature Cited

1. Burton S, Haggarty N, Harding D. One step purification of chymosin by mixed mode chromatography. *Biotechnol. Bioeng*. 1997;56:45–55.
2. Burton S, Harding D. Hydrophobic charge induction chromatography: salt independent protein adsorption and facile elution with aqueous buffers. *J. Chromatogr. A*. 1998;814:71–81.
3. Ghose S, Hubbard B, Cramer SM. Evaluation and comparison of alternatives to Protein A chromatography: mimetic and hydrophobic charge induction chromatographic stationary phases. *J. Chromatogr. A*. 2006;1122:144–152.
4. Zhao G, Sun Y. Displacement chromatography of proteins on hydrophobic charge induction adsorbent column. *J. Chromatogr. A* 2007; 1165:109–115.
5. Shi QH, Shen FF, Sun S. Studies of lysozyme binding to histamine as a ligand for hydrophobic charge induction chromatography. *Biotechnol. Progr*. 2010;26:134–141.
6. Guerrier L, Girot P, Schwartz W, Boschetti E. New method for the selective capture of antibodies under physiolgical conditions. *Bioseparation*. 2000;9:211–221.
7. Guerrier L, Flayeux I, Boschetti E. A dual-mode approach to the selective separation of antibodies and their fragments. *J. Chromatogr. B*. 2001;755:37–46.
8. Schwartz W, Judd D, Wysocki M, Guerrier L, Birck-Wilson E, Boschetti E. Comparison of hydrophobic charge induction chromatography with affinity chromatography on protein A for harvest and purification of antibodies. *J. Chromatogr. A*. 2001;908:251–263.
9. Boschetti E. Antibody separation by hydrophobic charge induction chromatography. *Trends Biotechnol*. 2002;20:333–337.
10. Tong H-F, Lin D-Q, Yuan X-M, Yao S-J. Enhancing IgG purification from serum albumin containing feedstock with hydrophobic charge-induction chromatography. *J. Chromatogr. A*. 2012;1244: 116–122.
11. Tong H-F, Lin D-Q, Gao D, Yuan X-M, Yao S-J. Caprylate as the albumin-selective modifier to improve IgG purification with hydrophobic charge-induction chromatography. *J. Chromatogr. A*. 2013; 1285:88–96.
12. Zhao G, Peng G, Li F, Shi Q, Sun Y. 5-Aminoindole, a new ligand for hydrophobic charge induction chromatography. *J. Chromatogr. A*. 2008;1211:90–98.

13. Chen J, Tetrault J, Ley A. Comparison of standard and new generation hydrophobic interaction chromatography resins in the monoclonal antibody purification process. *J. Chromatogr. A*. 2008;1177:272–281.
14. Xia H-F, Lin D-Q, Chen Z-M, Yao S-J. Salt-promoted adsorption of an antibody onto hydrophobic charge-induction adsorbents. *J. Chem. Eng. Data*. 2010;55:5751–5758.
15. Ghose S, Hubbard B, Cramer SM. Protein interactions in hydrophobic charge induction chromatography (HCIC). *Biotechnol. Progr*. 2005;21:498–508.
16. Zhao G, Dong X-Y, Sun Y. Ligands for mixed-mode protein chromatography: principles, characteristics and design. *J. Biotechnol*. 2009;144:3–11.
17. Zhang L, Sun Y. Molecular simulation of adsorption and its implications to protein chromatography: a review. *Biochem. Eng. J*. 2010; 48:408–415.
18. Xia H-F, Lin D-Q, Yao S-J. Hydrophobic charge induction chromatography: principles, characteristics and applications. *Chem. Ind. Eng. Prog*. 2010;29:1951–1956.
19. Zhou J, Chen S, Jiang S. Orientation of adsorbed antibodies on charged surfaces by computer simulation based on a united-residue model. *Langmuir*. 2003;19:3472–3478.
20. Zheng J, Li LY, Tsao, HK, Sheng YJ, Chen SF, Jiang SY. Strong repulsive forces between protein and oligo (ethylene glycol) self-assembled monolayers: a molecular simulation study. *Biophys. J*. 2005;89:158–166.
21. Zhou J, Thorpe IF, Izvekov S, Voth GA. Coarse-grained peptide modeling using a systematic multiscale approach. *Biophys. J*. 2007; 92:4289–4303.
22. He Y, Hower J, Chen SF, Bernards MT, Chang Y, Jiang SY. Molecular simulation studies of protein interactions with zwitterionic phosphorylcholine self-assembled monolayers in the presence of water. *Langmuir*. 2008;24:10358–10364.
23. Zhong T, Ai P, Zhou J. Structures and properties of PAMAM dendrimer: a multi-scale simulation study. *Fluid Phase. Equilibr* 2011; 302:43–47.
24. Xie Y, Zhou J, Jiang SY. Parallel tempering Monte Carlo simulations of lysozyme orientation on charged surfaces. *J. Chem. Phys*. 2010;132:065101.
25. Dong J, Zhou J. Solvent-responsive behavior of polymer-brush-modified amphiphilic gold nanoparticles. *Macromol. Theor. Simul*. 2013;22:174–186.
26. Liu J, Liao C, Zhou J. Multiscale simulations of protein G B1 adsorbed on charged self-assembled monolayers. *Langmuir*. 2013;29: 11366–11374.
27. Xie Y, Liao C, Zhou J. Effects of external electric fields on lysozyme adsorption by molecular dynamics simulations. *Biophys. Chem*. 2013;179:26–34.
28. Sun D, Zhou J. Ionic liquid confined in nafion: toward molecular-level understanding. *Aiche J*. 2013;59:2630–2639.
29. Liu J, Yu G, Zhou J. Ribonuclease A adsorption onto charged self-assembled monolayers: a multiscale simulation study. *Chem. Eng. Sci*. 2015;121:331–339.
30. Peng C, Liu J, Zhao D, Zhou J. Adsorption of hydrophobin on different self-assembled monolayers: the role of the hydrophobic dipole and the electric dipole. *Langmuir*. 2014;30:11401–11411.
31. Zhao D, Peng C, Zhou J. Lipase adsorption on different nanomaterials: a multi-scale simulation study. *Phys. Chem. Chem. Phys*. 2015; 17:840–850.
32. Latour RA. Molecular simulation of protein-surface interactions: benefits, problems, solutions, and future directions (Review). *Biointerphases*. 2008;3:FC2–FC12.
33. Wang H-Y, Lin D-Q, Yao S-J, Yun J-X, Yao K-J. Molecular simulation of the interactions between 4-mercaptoethyl-pyridine ligand and IgG. *Acta Chim. Sinica*. 2010;68:1597–1602.
34. Lin D-Q, Tong H-F, Wang H-Y, Yao S-J. Molecular insight into the ligand–IgG interactions for 4-mercaptoethyl-pyridine based hydrophobic charge-induction chromatography. *J. Phys. Chem. B*. 2012; 116:1393–1400.
35. Lin D-Q, Tong H-F, Wang H-Y, Shao S, Yao S-J. Molecular mechanism of hydrophobic charge-induction chromatography: interactions between the immobilized 4-mercaptoethyl-pyridine ligand and IgG. *J. Chromatogr. A*. 2012;1260:143–153.
36. Zhang L, Zhao G, Sun Y. Molecular insight into protein conformational transition in hydrophobic charge induction chromatography: a molecular dynamics simulation. *J. Phys. Chem. B*. 2009;113: 6873–6880.
37. Zhang L, Zhao G, Sun Y. Molecular dynamics simulation and experimental validation of the effect of pH on protein desorption in hydrophobic charge induction chromatography. *Mol. Simulat*. 2010; 36:1096–1103.
38. Zhang L, Zhao G, Sun Y. Effects of ligand density on hydrophobic charge induction chromatography: molecular dynamics simulation. *J. Phys. Chem. B* 2010;114:2203–2211.
39. Zhang L, Bai S, Sun Y. Modification of Martini force field for molecular dynamics simulation of hydrophobic charge induction chromatography of lysozyme. *J. Mol. Graph. Model*. 2011;29: 906–914.
40. Wei T, Carignano MA, Szleifer I. Lysozyme adsorption on polyethylene surfaces: why are long simulations needed? *Langmuir*. 2011; 27:12074–12081.
41. Wei T, Carignano MA, Szleifer I. Molecular dynamics simulation of lysozyme adsorption/desorption on hydrophobic surfaces. *J. Phys. Chem. B*. 2012;116:10189–10194.
42. Yu G, Liu J, Zhou J. Mesoscopic coarse-grained simulations of lysozyme adsorption. *J. Phys. Chem. B*. 2014;118:4451–4460.
43. Marrink SJ, Risselada HJ, Yefimov S, Tieleman DP, de Vries AH. The MARTINI force field: coarse grained model for biomolecular simulations. *J. Phys. Chem. B*. 2007;111:7812–7824.
44. Monticelli L, Kandasamy SK, Periole X, Larson RG, Tieleman DP, Marrink S-J. The MARTINI coarse-grained force field: extension to Proteins. *J. Chem Theory Comput*. 2008;4:819–834.
45. Wu Z, Cui QA, Yethiraj A. A new coarse-grained model for water: the importance of electrostatic interactions. *J. Phys. Chem. B* 2010; 114:10524–10529.
46. Wu Z, Cui Q, Yethiraj A. a new coarse-grained force field for membrane-peptide simulations. *J. Chem Theory Comput*. 2011;7: 3793–3802.
47. Fumi FG, Tosi MP. Ionic sizes and born repulsive parameters in the NaCl-type alkali halides I: the Huggins-Mayer and Pauling forms. *J. Phys. Chem. Solids*. 1964;25:31–43.
48. Tosi MP, Fumi FG. Ionic sizes and born repulsive parameters in the NaCl-type alkali halides II: the generalized Huggins-Mayer form. *J. Phys. Chem. Solids*. 1964;25:45–52.
49. Essmann U, Perera L, Berkowitz ML, Darden T, Hsing L, Pedersen L. G. A smooth particle mesh Ewald method. *J. Chem. Phys*. 1995; 103:8577–8593.
50. Darden T, Pearlman D, Pedersen LG. Ionic charging free energies: spherical versus periodic boundary conditions. *J. Chem. Phys*. 1998; 109:10921–10935.
51. Sun Y, Welsh WJ, Latour RA. Prediction of the orientations of adsorbed protein using an empirical energy function with implicit solvation. *Langmuir*. 2005;21:5616–5626.
52. Dismer F, Petzold M, Hubbuch J. Effects of ionic strength and mobile phase pH on the binding orientation of lysozyme on different ion-exchange adsorbents. *J. Chromatogr. A*. 2008;1194:11–21.
53. Tiemeyer S, Paulus M, Tolan M. Effect of surface charge distribution on the adsorption orientation of proteins to lipid monolayers. *Langmuir*. 2010;26:14064–14067.
54. Periole X, Marrink S-J. The Martini coarse-grained force field. In: Monticelli L, Salonen E, editors. *Biomolecular Simulations*, Vol. 924. New York: Humana Press, 2013:533–565.
55. Periole X, Cavalli M, Marrink SJ, Ceruso MA. Combining an elastic network with a coarse-grained molecular force field: structure, dynamics, and intermolecular recognition. *J. Chem Theory Comput*. 2009;5:2531–2543.
56. Dolinsky TJ, Nielsen JE, McCammon JA, Baker NA. PDB2PQR: an automated pipeline for the setup of Poisson-Boltzmann electrostatics calculations. *Nucleic Acids. Res*. 2004; 32:W665–W667.
57. Hess B, van Der Spoel D, Lindahl E. *Gromacs User Manual Version 4.5.4*. Netherland: University of Groningen, 2010.
58. Yesylevskyy SO, Schafer LV, Sengupta D, Marrink SJ. Polarizable water model for the coarse-grained MARTINI force field. *Plos Comput. Biol*. 2010;6:e1000810.
59. Berendsen HJC, Postma JPM, van Gunsteren WF, DiNola A, Haak JR. Molecular dynamics with coupling to an external bath. *J. Chem. Phys*. 1984;81:3684–3690.
60. Humphrey W, Dalke A, Schulten K. VMD: visual molecular dynamics. *J. Mol. Graph*. 1996;14:33–38.
61. Pettersen EF, Goddard TD, Huang CC, Couch GS, Greenblatt DM, Meng EC, Ferrin TE. UCSF Chimera-A visualization system for exploratory research and analysis. *J. Comput. Chem*. 2004;25: 1605–1612.

62. Sigal GB, Mrksich M, Whitesides GM. Effect of surface wettability on the adsorption of proteins and detergents. *J. Am. Chem. Soc*. 1998;120:3464–3473.
63. Chen X, Yang T, Kataoka S, Cremer PS. Specific ion effects on interfacial water structure near macromolecules. *J. Am. Chem. Soc*. 2007;129:12272–12279.
64. Feng H, Zhou J, Lu X. Molecular dynamics simulations on the interfacial structures of electrolyte solutions. *Acta Chim. Sinica*. 2009;67:2407–2412.
65. Feng H, Zhou J, Lu X, Fichthorn KA. Communication: molecular dynamics simulations of the interfacial structure of alkali metal fluoride solutions. *J. Chem. Phys*. 2010;133: 061103.
66. Zhou J, Lu X, Wang Y, Shi J. Molecular dynamics study on ionic hydration. *Fluid. Phase. Equilibr*. 2002;194–197:257–270.

Manuscript received Nov. 12, 2014, and revision received Mar. 17, 2015.